
STELLAR ORBITS IN DOUBLY BARRED GALAXIES

H. HASAN

Astrophysics Division, NASA Headquarters, Washington D.C. 20546

and

Jet Propulsion Lab., California Institute of Technology, 4800 Oak Grove

Dr., Pasadena CA 91109

1 Introduction

The **question** of bars within bars has been reviewed by Friedli and Martinet (1993), who have also performed N-body simulations to produce nested bars. They propose that if a system of embedded bars is effective in transporting gas to the galactic center (Shlosman et al. 1989), then it is perhaps a step in the secular evolution of barred galaxies. In order to pursue this interesting proposition, and also because observational evidence for the existence of secondary bars is mounting (e.g. Buta & Crocker, 1993; Shaw et al., 1993, Wozniak et al. 1994), it is important to understand the stellar kinematics in such Systems.

As a first step in this direction, we compute stellar orbits in a two dimensional potential representing the galaxy and examine surfaces of section (s.o.s.) in the galactic plane. We consider the secondary bar to rotate at the same pattern speed and to be (a) parallel and (b) perpendicular to the primary bar. In each case we study the effect of increasing the mass of the secondary bar and of changing its width. We find that increasing the mass of the secondary bar causes the appearance of resonances, particularly for the perpendicular bar, when there is a rich resonance structure in the surface of section. The effect of the resonances is, of course, to destabilize the B (or x_1) orbits which support the bar. The effect of the inner bar in this sense is similar to that of a spherical central mass, the growth of which causes bar destruction (Hasan & Norman 1990). A similar effect is seen when we keep the mass of the secondary bar constant, but make it more concentrated by reducing its width (cf. Hasan et al. 1993 for the spherical central mass case). An interesting difference we observe in the surfaces of section of the case of a spherical central mass and an inner bar is, that in the latter case increasing the central mass produces resonance structures on the retrograde side as well. In the former case, retrograde orbits were not strongly affected by a growth of a central mass (Hasan et al. 1993).

We propose to follow up this study by computing periodic orbits in a three dimensional model potential and also for the more interesting case of two bars inclined at an arbitrary angle and rotating at different pattern speeds.

2 Formulation

The galactic potential is approximated by

$$V = V_c + V_{b_1} + V_{b_2} \quad (1)$$

where V_c , representing the axisymmetric central (disk) component, is modelled by a Plummer sphere

$$V_c = -GM_c / \sqrt{(A_c^2 + R^2)} \quad (2)$$

Here A_c is the length scale of the sphere, G , the gravitational constant and M_c , the total mass of the sphere. An inhomogeneous prolate bar with density distribution

$$\rho = \begin{cases} \rho_0(1 - m^2)^2 & \text{if } m < 1 \\ 0 & m > 1 \end{cases} \quad (3)$$

where

$$m^2 = \frac{x'^2}{a^2} + \frac{y'^2}{b^2} + \frac{z^2}{c^2} \quad (4)$$

with $a > b, b = c$, is chosen to model the components V_{b_i} of the potential. We consider orbits in the galactic plane corotating with the bars (both bars are considered to have the same pattern speed).

The free parameters of this potential are as follows.

1. The relative mass ratio of the bars M_{b_i}/M_T , where $M_T = M_{b_1} + M_{b_2} + M_c$.
2. The semi-major axes of the bars, a_i .
3. The bar axial ratios, b_i/a_i .
4. The ratio of the length scale of the central component to the length of the bar, A_c/a_1 .
5. The ratio of the coronation radius to the length of the primary bar, R_{cr}/a_p , or equivalently the pattern speed, Ω_p .

For normalization purposes it is found convenient to fix the primary bar semi-major axis a_1 at 9 kpc, and the total mass $M_T = 4.67 \times 10^{10} M_\odot$ (Hasan and Norman, 1990). For all cases studied this normalization results in a pattern speed $\Omega_p \sim 15$ km/sec/kpc so that $R_{cr}/a_1 = 1$. The parameters fixed for all calculations are: the primary bar mass, $M_{b_1}/M_T = 0.3$, its semi-minor axis, $b_1 = 4.05$ kpc, secondary bar major axis, $a_2 = 1.8$ kpc and the length scale of the central component, $A_c/a_1 = 0.5$. The Jacobi constant was fixed so that a star could reach a maximum distance corresponding to the edge of the minor axis of the primary bar. The minor axis of the secondary bar was fixed to $0.45a_2 = 0.81$ kpc.

3 Discussion of results

We examined the effect of the secondary bar on the orbits of this potential for four sets of conditions.

1. *Secondary bar parallel to primary bar and mass varied.* As the mass of the secondary bar was varied, the core mass was allowed to vary so that the total mass remained constant.

2. *Secondary bar perpendicular to primary bar and mass varied.* Same as above except for the orientation of the secondary bar.
3. *Secondary bar parallel to primary bar and its axial ratio varied.* The value of b_2/a_2 was changed from 0.45 to 0.35, 0.25, while the mass was fixed at $M_{b_2}/M_T = 0.05$.
4. *Secondary bar perpendicular to primary bar and its axial ratio varied.* Same as above except for the orientation of the secondary bar.

3.1 Variation of secondary bar mass

Orbits were computed by solving the equations of motion numerically using a seventh-order Runge Kutta scheme. Stars were launched along the y -axis with velocities parallel to the positive x -axis, and surfaces of section plots made by storing the values of (y, \dot{y}) every time the star crossed the y -axis with a positive value of x .

3.1.1 Secondary bar parallel to primary bar

An examination of the surfaces of section for this case (which we shall refer to as case I) are shown in Figure 1. From the figure we see that in the presence of a small secondary bar ($M_{b_2}/M_T = 0.05$) the direct orbits which support the bar (the B or x_1 orbits) fill almost all the space available to direct orbits (RHS of surfaces of section in the figures). As the mass of the secondary bar increases the interaction of the primary and secondary bars causes the appearance of resonances, represented by islands, both on the direct and retrograde sides. Further, the region of stochasticity increases and the phase space occupied by B orbits shrinks, thus causing a weakening of the primary bar. Nevertheless, the primary bar is not destroyed till the secondary bar is quite massive ($\sim 20\%$ of the total mass). Particularly noticeable is a minor orbit family, which starts breaking off from the B family, when $M_{b_2}/M_T = 0.11$, and appears in the surface of section diagram as a protrusion in the oval invariant curve. As the M_{b_2} grows, the minor family strengthens and appears as a distinct island of curves lying between the retrograde and direct orbit families. In our earlier analyses of spherical central masses (Hasan et al. 1993) we saw that this family of “banana” orbits or “looplets” takes stars outside the galactic plane and helps populate the bulge.

3.1.2 Secondary bar perpendicular to primary bar

The surfaces of section for this case (referred to as case II) have been plotted along side the earlier case (of the secondary bar parallel to primary bar) for purposes of comparison. The general behavior of the s.o.s is similar in both cases. However, the minor orbit family appears for smaller masses, $M_{b_2}/M_T \approx 0.07$ and has disappeared once the mass has grown to $M_{b_2}/M_T = 0.09$. For still heavier secondary bars, the invariant curves representing B orbits change from an oval shape to a more rectangular to a diamond shape, indicating that the influence of the secondary bar is stronger, and the galaxy will get a boxier shape. The orbits are still elongated along the primary bar, but develop complicated looped shapes as higher order resonances set in. Stochasticity along both bars increases and eventually both bars will be destroyed.

3.1.3 Role of resonances in bar destruction

Physical insight may be gained by looking at the frequency curves for each case. These are shown in Fig.2 for two cases. In each case curves are plotted for the angular velocities Ω_x and Ω_y along x and y respectively and the corresponding curves for $\Omega_x - \kappa_x/2$ and $\Omega_y - \kappa_y/2$, where κ represents the “epicyclic frequency” given by

$$\kappa_{x(y)}^2 = V_{xx} - \frac{v}{u} + 2\Omega_{x(y)} \quad (5)$$

with

$$\Omega_{x(y)}^2 = V_{x(y)}/x(y) \quad (6)$$

Here V_x, V_y represent partial derivatives of the potential with respect to x and y respectively and V_{xx}, V_{yy} are the corresponding second derivatives.

For all cases considered here, the pattern speed, Ω_p , is lower than the peak in the curves $\Omega - \kappa/2$, indicating the presence of Inner Lindblad Resonances (I I, R). For the case of the parallel bars (case 1) there are two ILRs corresponding to the two bars. Between the potential center and the first ILR, and the second ILR and coronation, orbits will be parallel and support bars, while in the in between region, orbits will be antialigned to the bar. As the secondary bar mass increases in mass, the outer ILR moves closer to the coronation radius, thus reducing the phase space available to orbits supporting the primary bar, which eventually gets destroyed. At the same time, the inner ILR moves closer to the potential center, reducing the phase space available to the secondary bar and causing its destruction.

For the case of the perpendicular bars (case H), only the outer ILR is present. The orbits close to the potential center are antialigned, thus supporting the secondary bar. With increase in mass of the secondary bar, as in case I, the outer ILR moves outwards and the bar is eventually destroyed.

3.2 Variation of secondary bar axial ratio (b_2/a_2)

The problem was re-examined in another complementary scheme. This time the mass, M_{b_2}/MT , of the secondary bar was fixed at 0.05, and was concentrated more and more inside the bar by changing the axial ratio, $b_2/a_2 = 0.45, 0.35, 0.25$, holding all other parameters constant. Some examples of surfaces of section are shown in Figure 3. As expected from our earlier studies (Hasan et al. 1993), a thinner and more concentrated secondary bar causes more stochasticity than a thicker, less dense bar. In case II, for $b_2/a_2 = 0.25$, some of the B orbits are converted to A orbits, which manifest themselves in the s.o.s. as islands along the edges of the s.o.s. along the zero velocity curve,

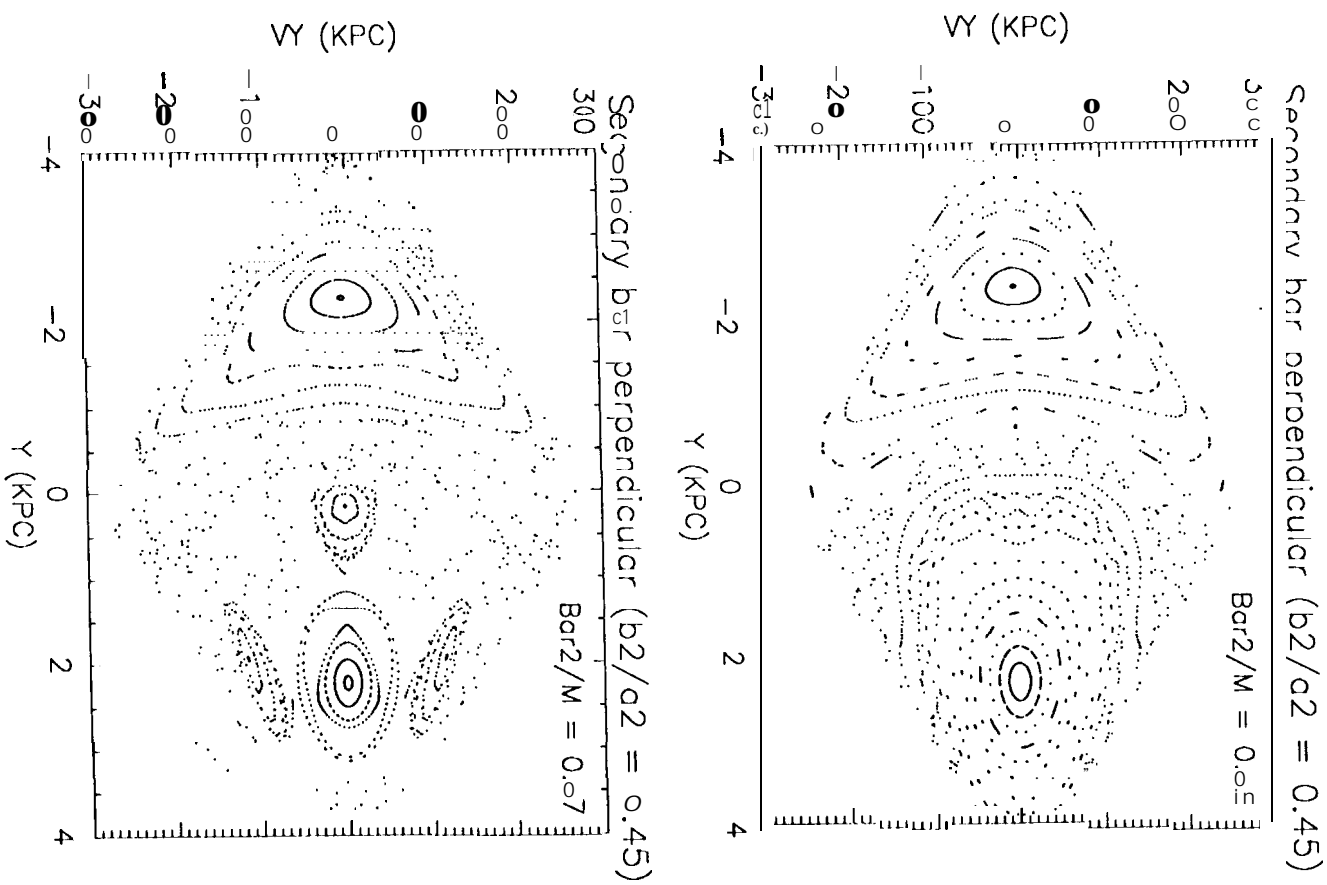
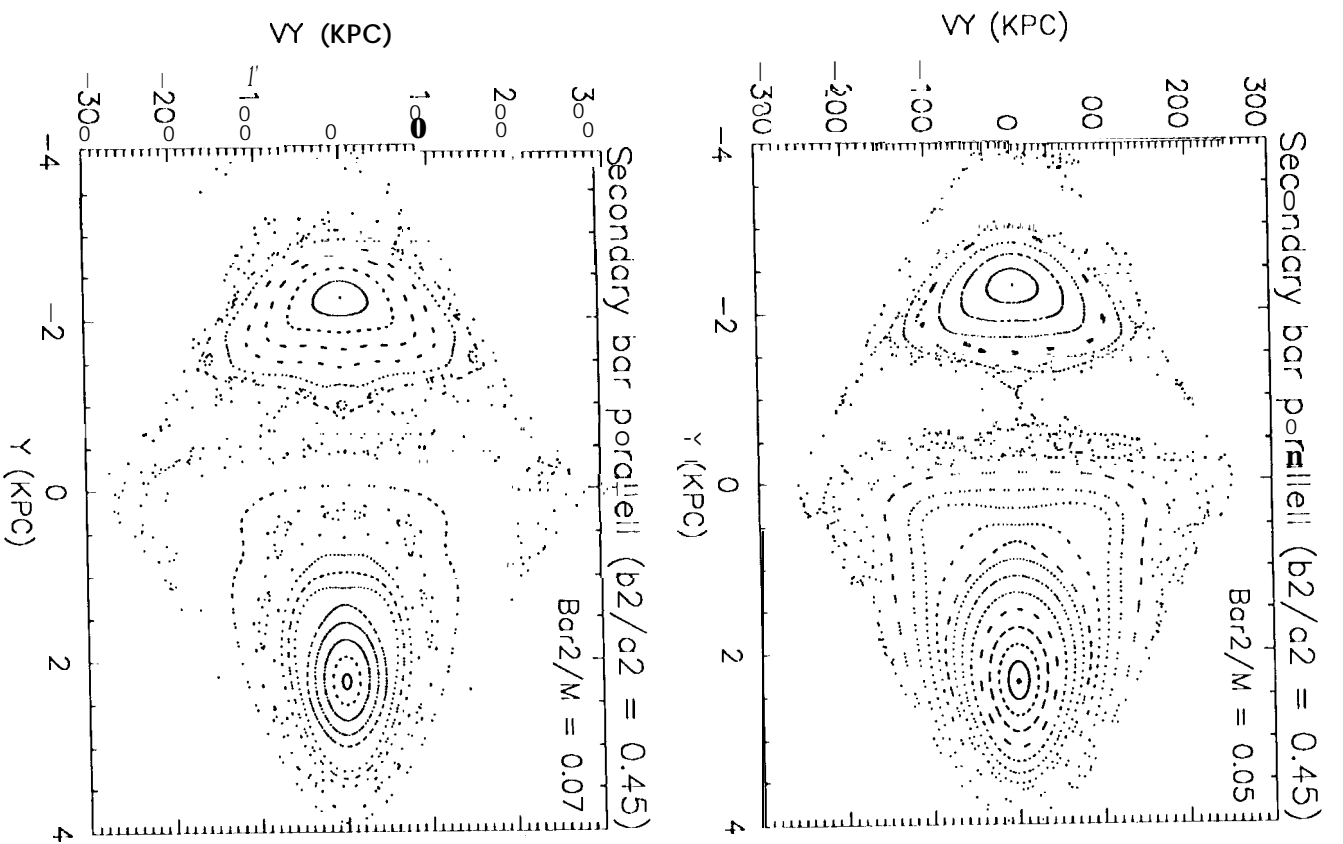
4 Summary

In the case of two bars rotating with the same pattern speed, the influence of a secondary bar on stellar orbits in a barred galaxy is to destabilize them and to weaken and eventually destroy both bars. A small secondary bar can retain its identity, but as it increases in mass, it will shrink in size, as will the primary. This behavior is interpreted as an interplay between the natural resonance frequencies of the bars and the appearance and outward movement of an outer ILR and, in case I, also the inward movement of an inner ILR.

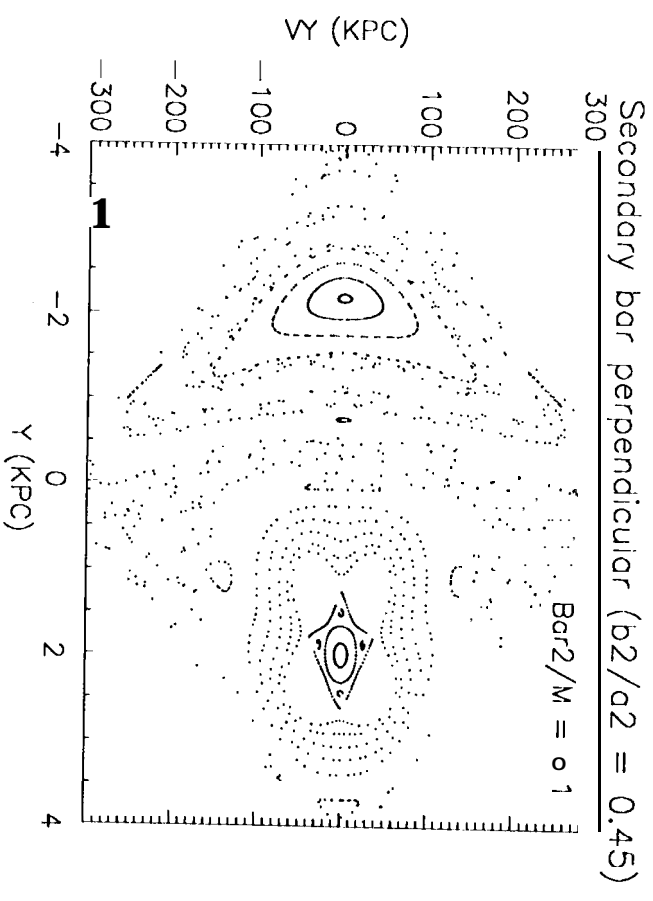
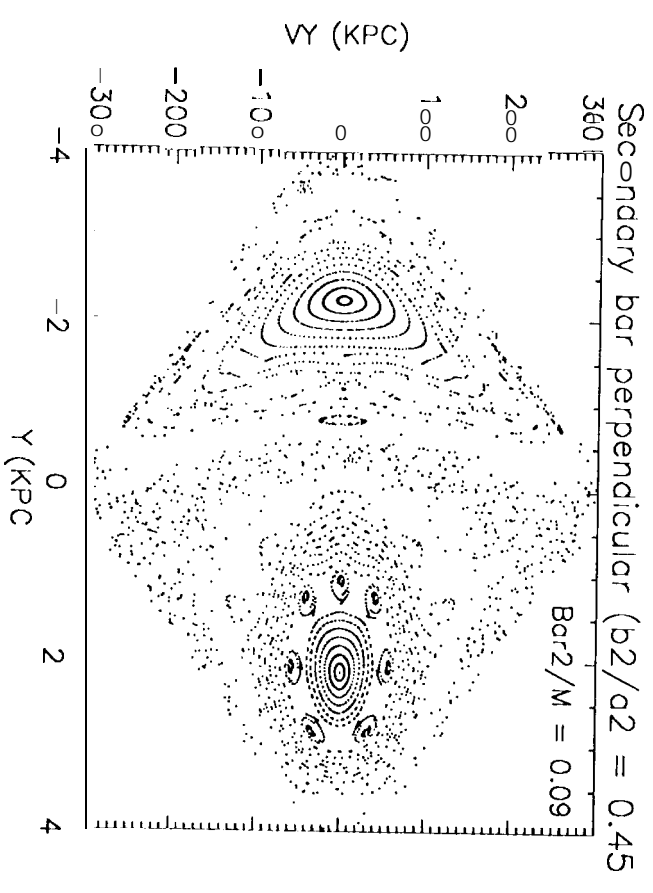
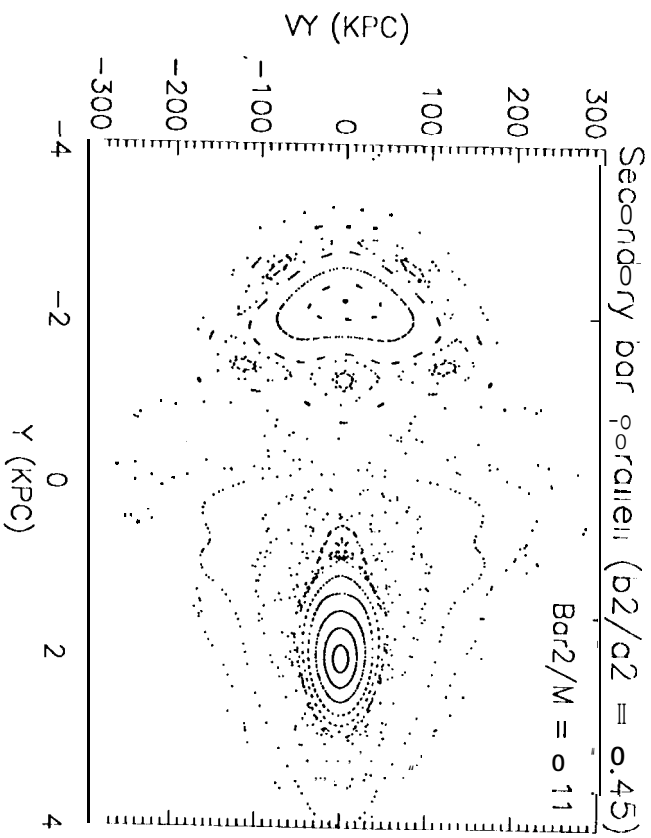
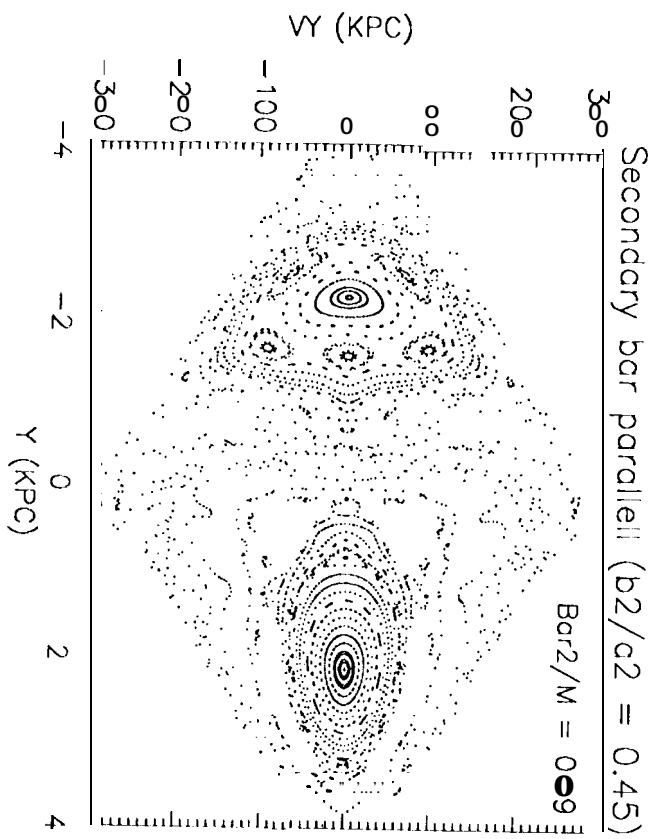
A more detailed study of periodic orbits in a three dimensional potential is under way to characterize the orbits and examine the effect of inner bars and rings on motion out of the galactic plane. orbits for bars rotating at different pattern speeds and arbitrary angles will also be examined in the future,

References

1. Buta R. and Crocker, D. A. 1993, AJ 105, 1344.
2. Friedli, D. and Martinet, L. 1993, A&A 277,27.
3. Hasan, H. and Newman, C. 1990, ApJ 361,69.
4. Hasan, H., Pfenniger, D. and Norman, C. 1993, ApJ 409,91.
5. Shlosman, I., Frank, J. and Begelman, M. C. 1989, Nature 338, 45.
6. Shaw, M. A., Combes, F., Axon, D. J. and Wright, G. G. 1993, A&A 273,31.
7. Wozniak, H., Friedli, D., Martinet, L., Martin, P. and Bratschi, P. 1994, A&A



Fig



Fig

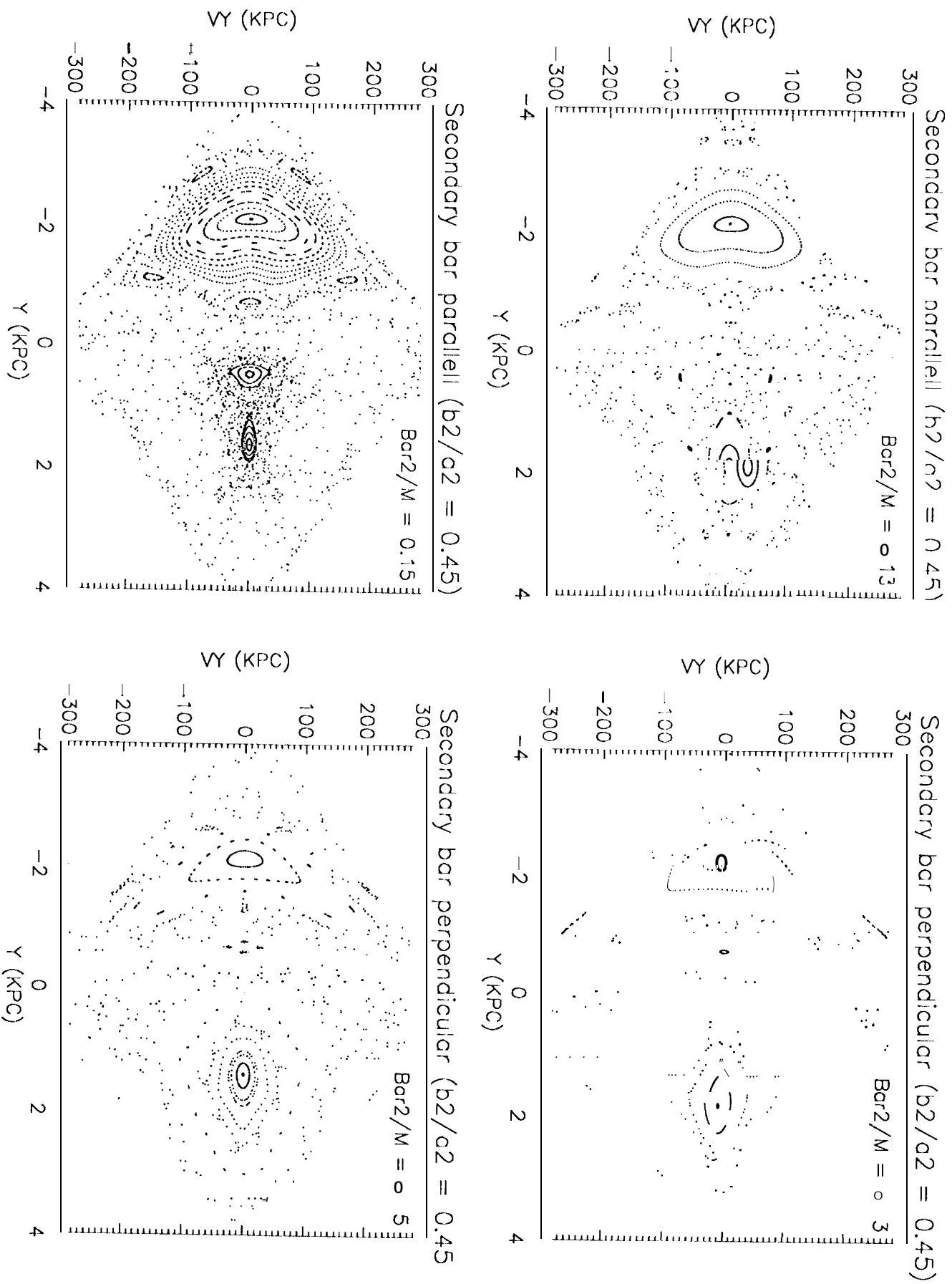


Fig. 1

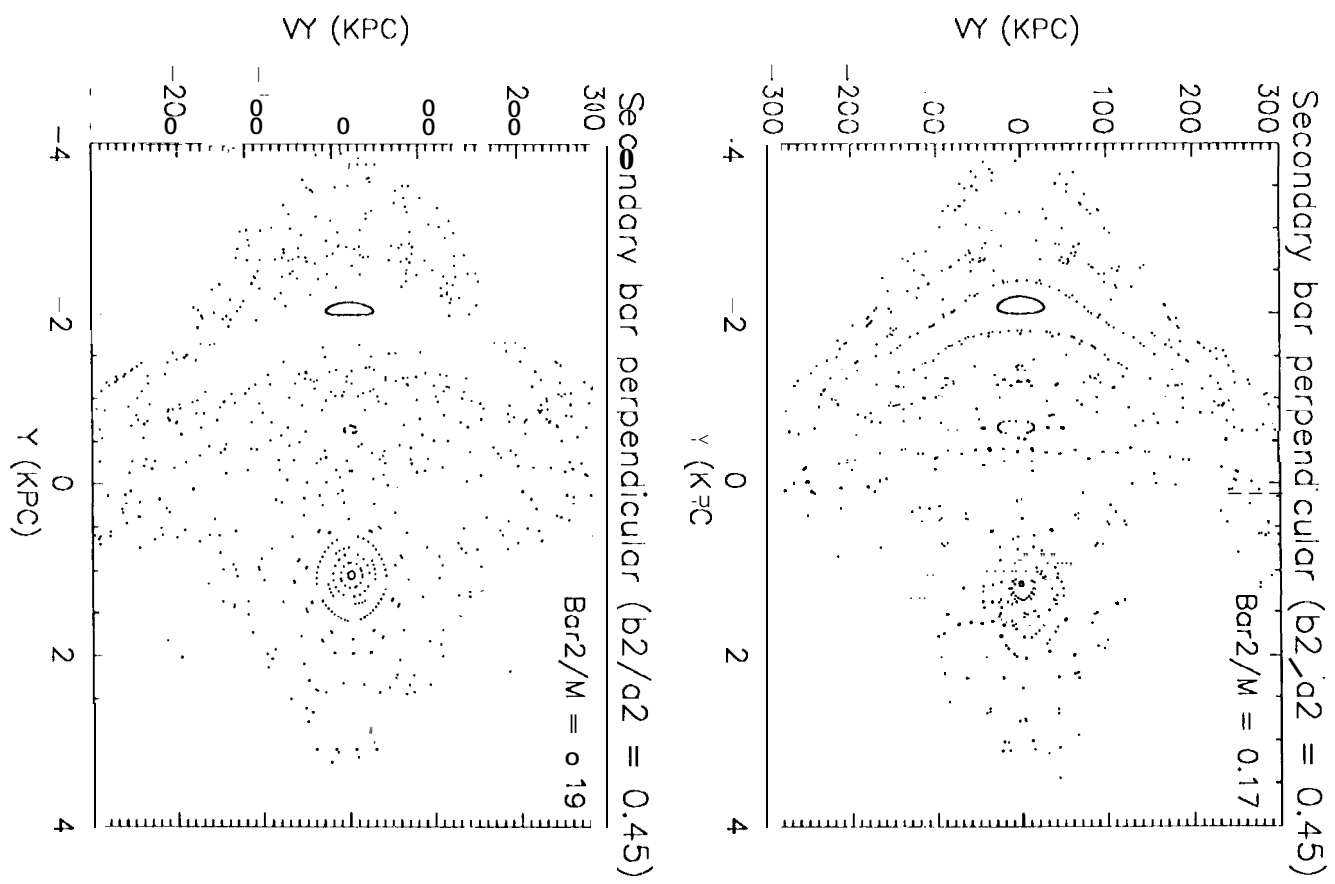
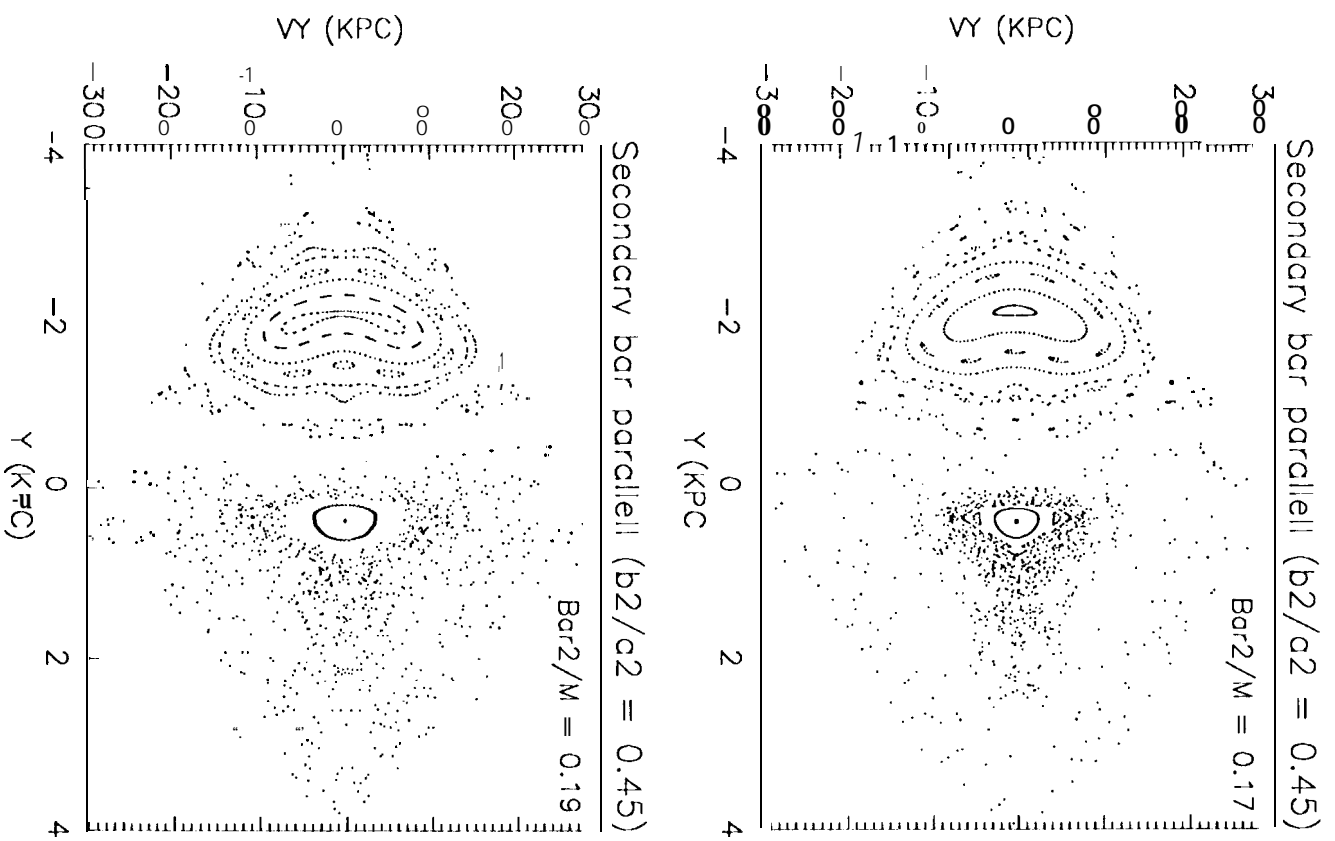
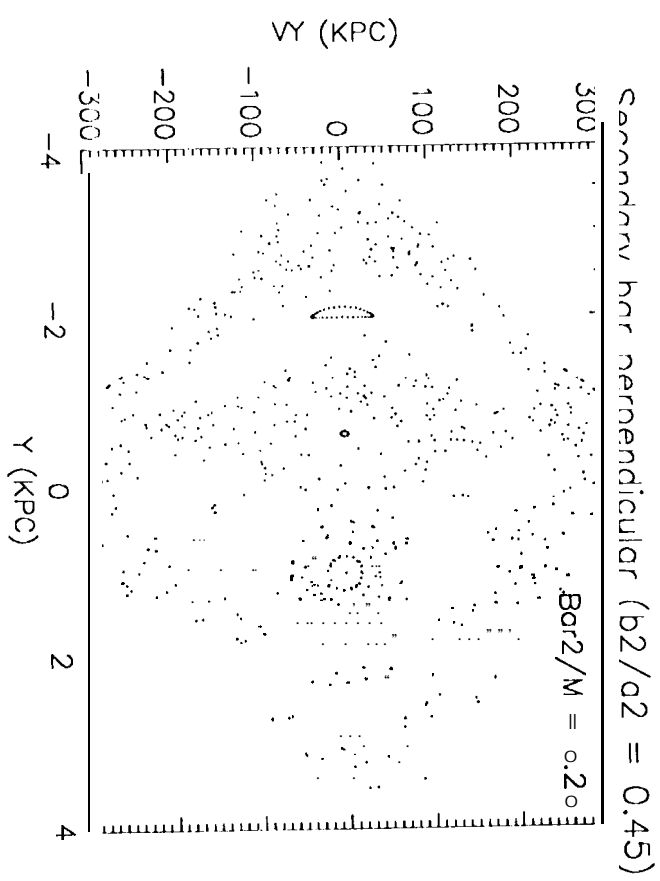
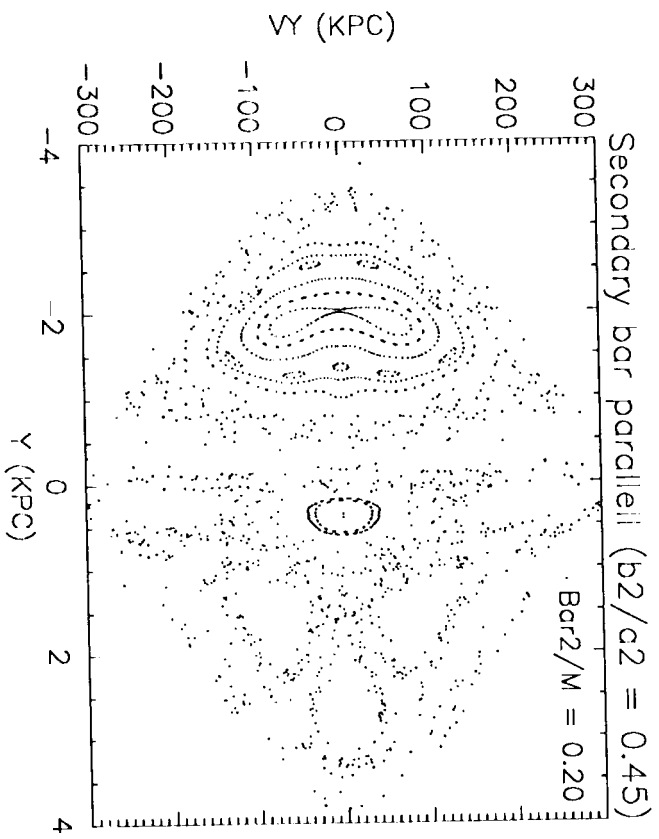


Fig 1



Fig

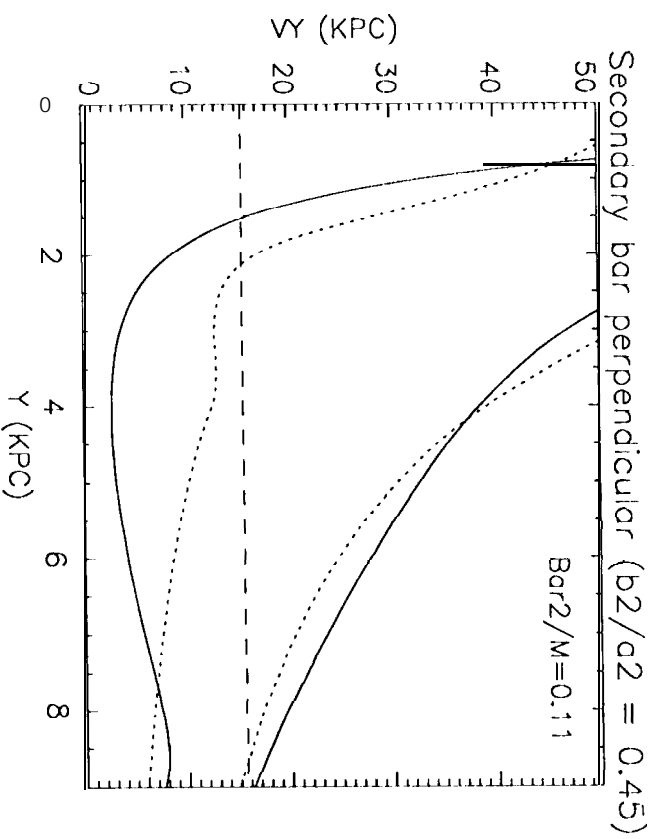
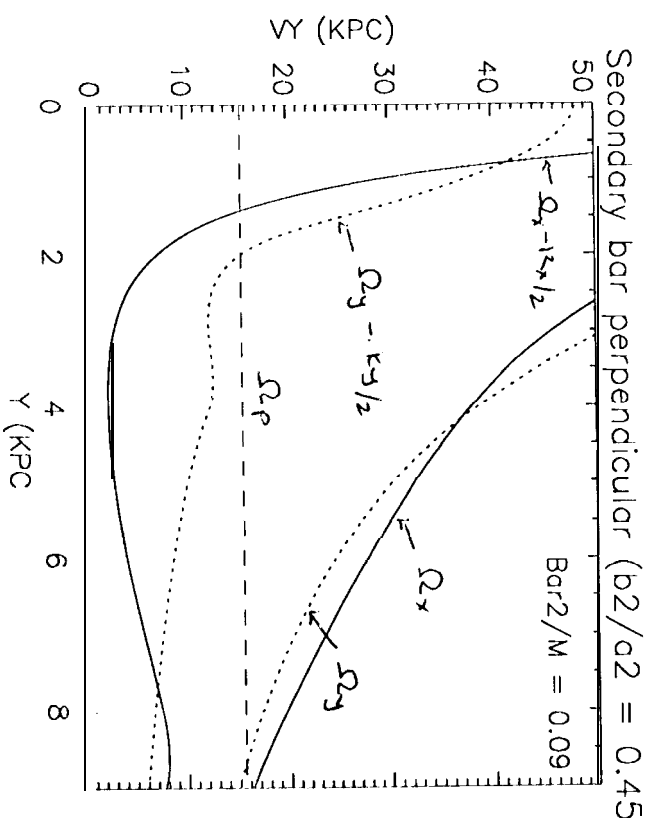
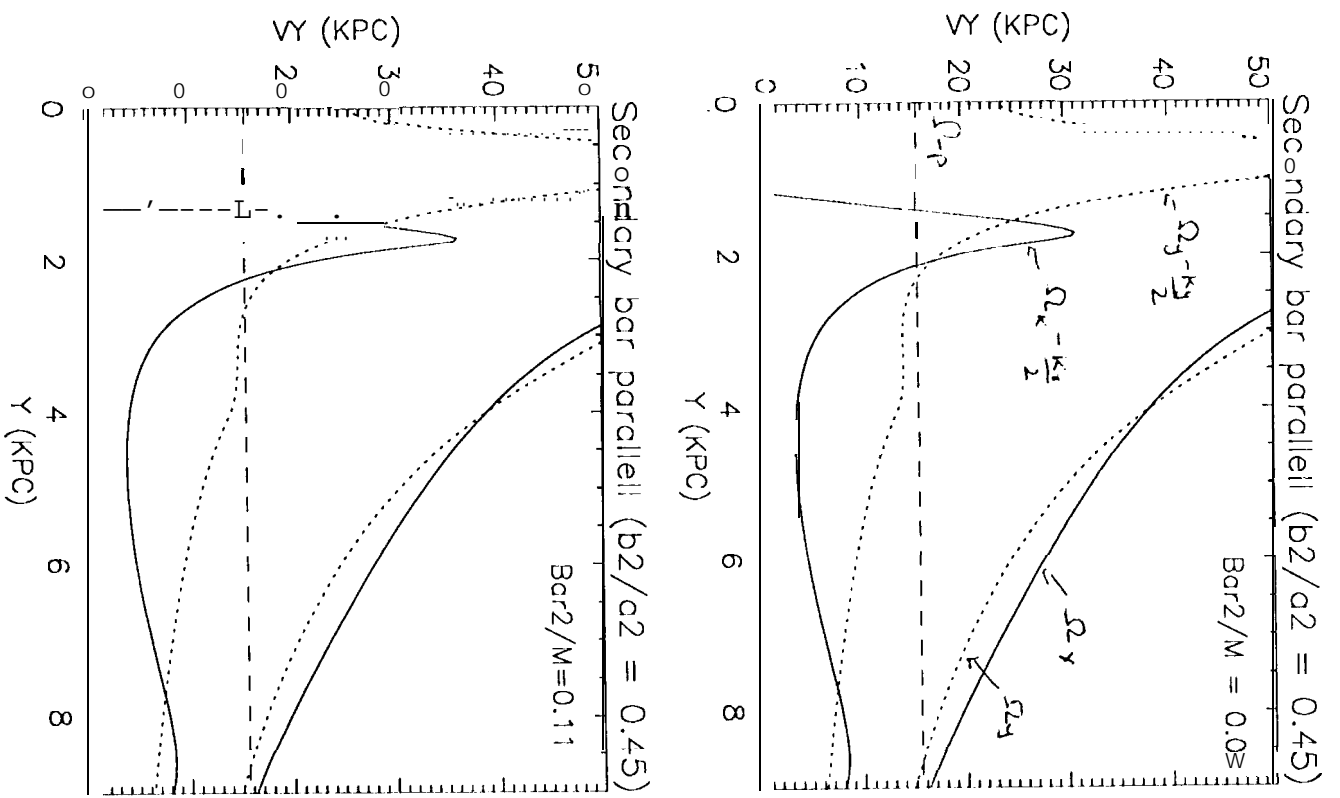
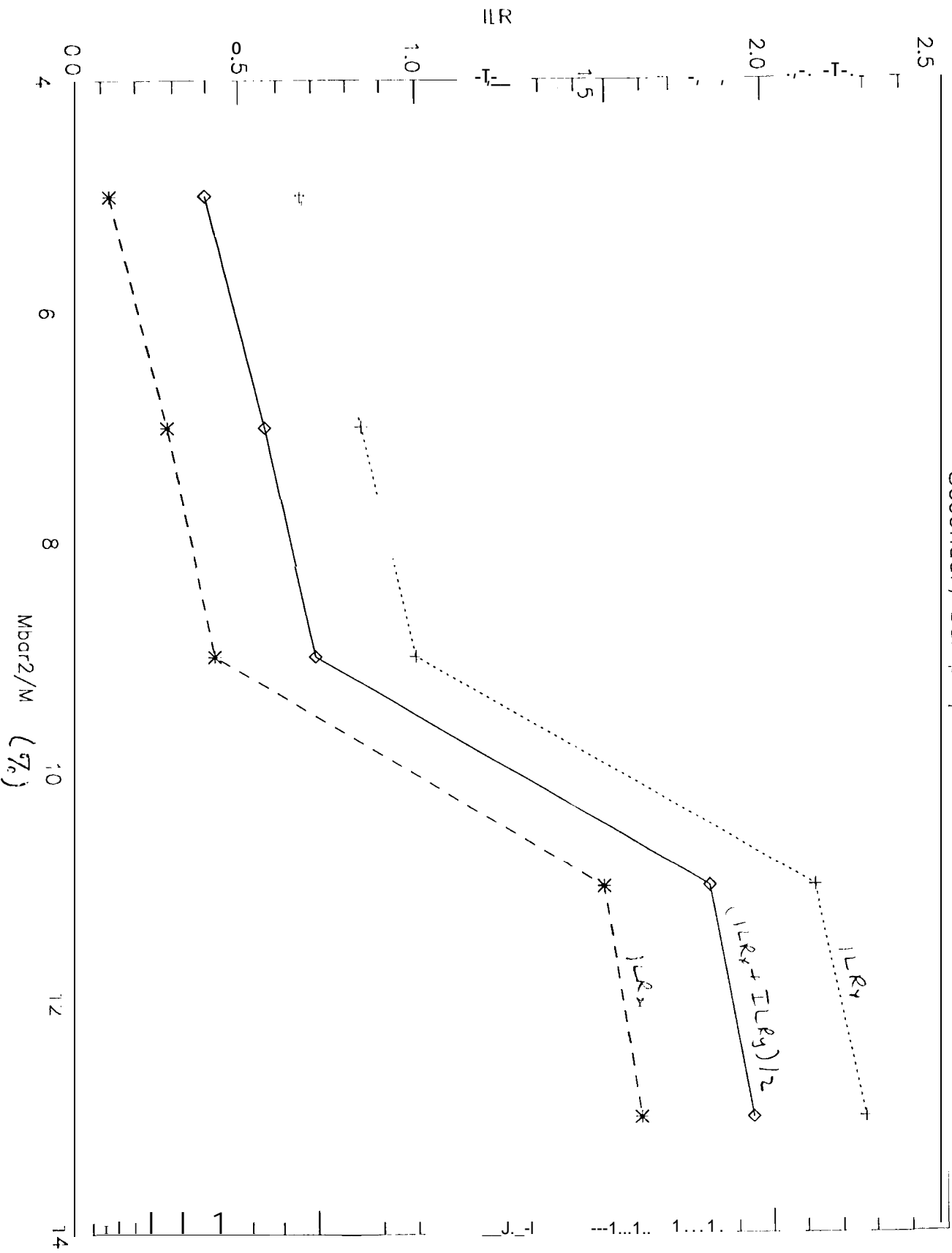
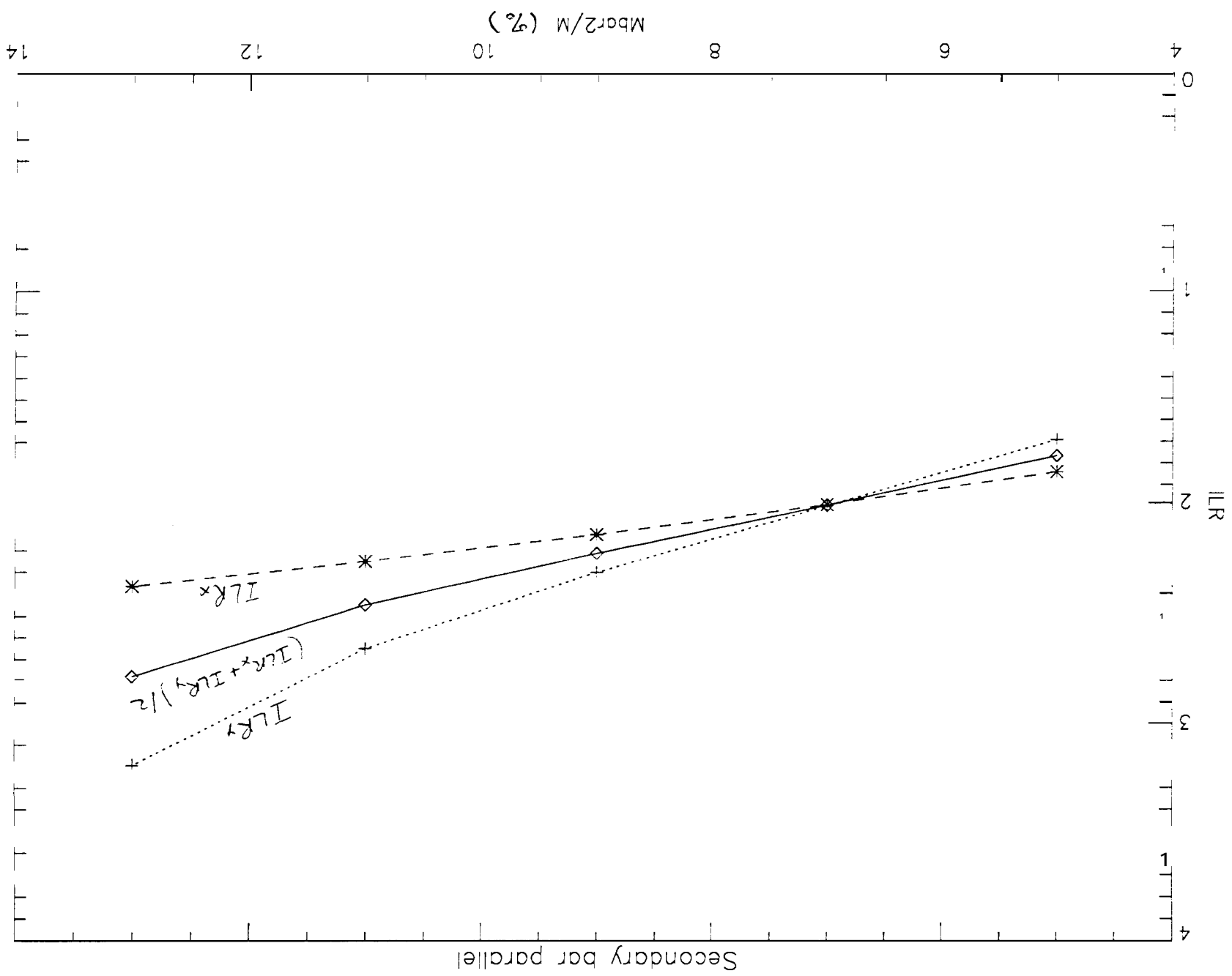


Fig. 2

Secondary bar perpendicular





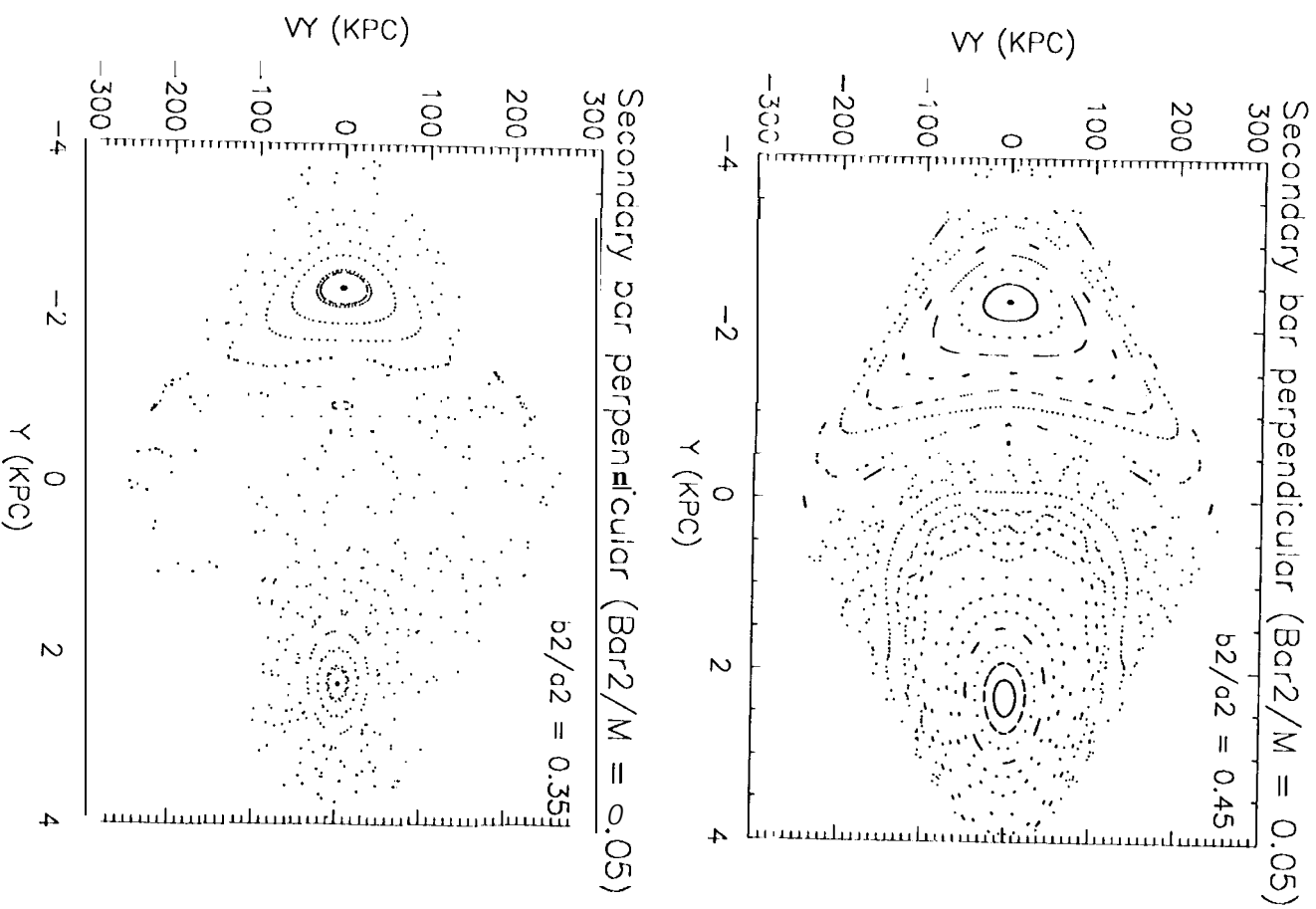
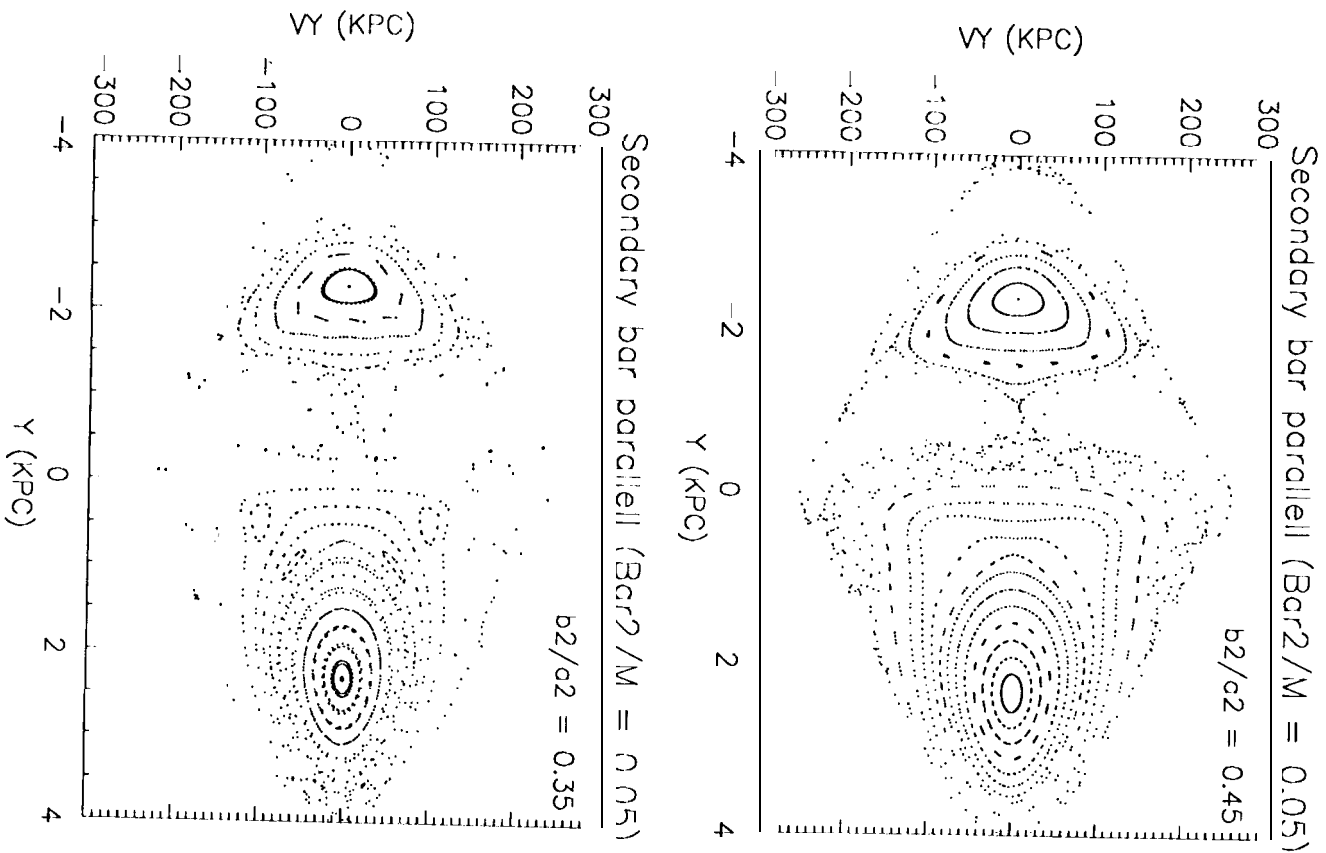


Fig. 3

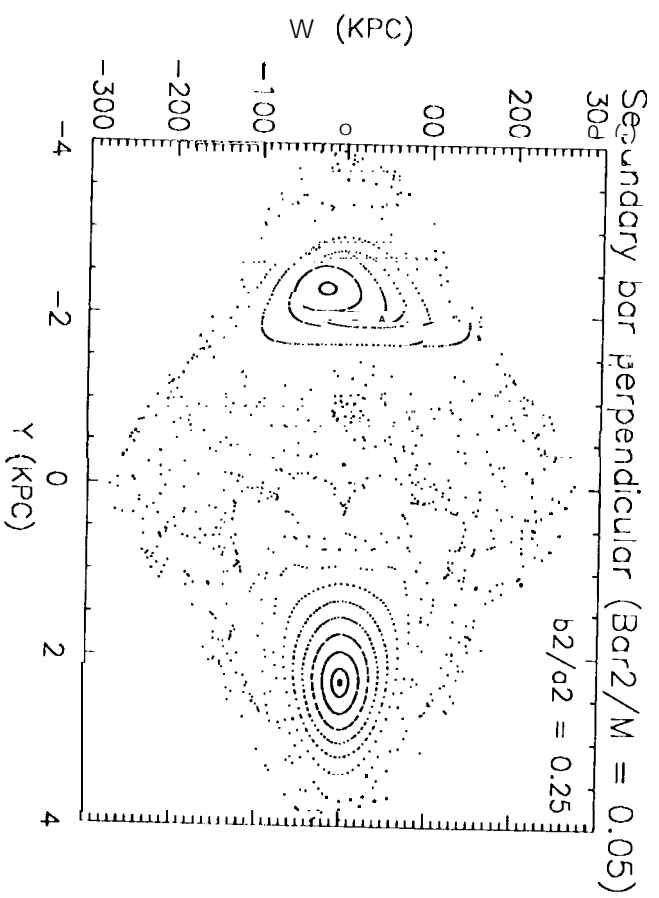
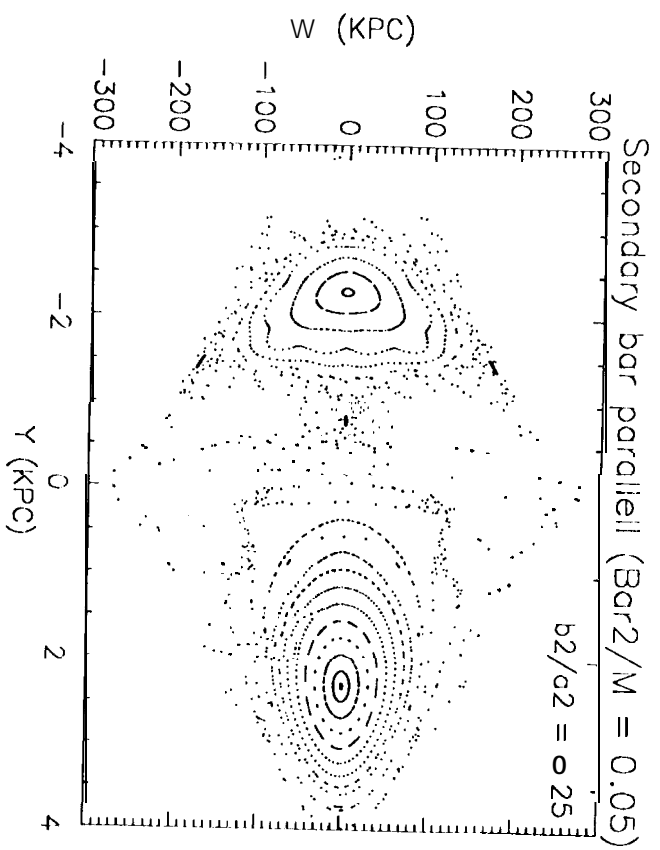


Fig. 3